Nonperturbative renormalization of domain wall fermions: Quark bilinears

T. Blum,[1] N. Christ,[2] C. Cristian,[2] C. Dawson,[3] G. Fleming,[2,*] G. Liu,[2] R. Mawhinney,[2] A. Soni,[3] P. Vranas,[4] M. Wingate,[1,*] L. Wu,[2] and Y. Zhestkov[2]

[1]*RIKEN BNL Research Center, Brookhaven National Laboratory, Upton, New York 11973*
[2]*Physics Department, Columbia University, New York, New York 10027*
[3]*Physics Department, Brookhaven National Laboratory, Upton, New York 11973*
[4]*IBM T. J. Watson Research Center, Yorktown Heights, New York 10598*

We find the renormalization coefficients of the quark field and the flavor nonsinglet fermion bilinear operators for the domain wall fermion action, in the regularization independent (RI) renormalization scheme. Our results are from a quenched simulation, on a $16^3 \times 32$ lattice, with $\beta = 6.0$ and an extent in the fifth dimension of 16. We also discuss the expected effects of the residual chiral symmetry breaking inherent in a domain wall fermion simulation with a finite fifth dimension, and study the evidence for both explicit and spontaneous chiral symmetry breaking effects in our numerical results. We find that the relations between different renormalization factors predicted by chiral symmetry are, to a good approximation, satisfied by our results and that systematic effects due to the (low energy) spontaneous chiral symmetry breaking and zero modes can be controlled. Our results are compared against the perturbative predictions for both their absolute value and renormalization scale dependence.

I. INTRODUCTION

Renormalization of lattice operators is an essential ingredient needed to deduce physical results from numerical simulations. In contrast with the determination of hadronic masses, physical matrix elements can be determined only if the normalization of the appropriate lattice operators can be related to that of the corresponding continuum operators, conventionally specified perturbatively at short distances. In principle, lattice perturbation theory may be used to establish this connection. However, lattice perturbation theory converges slowly and the expansion parameter, the square of the lattice coupling evaluated at the lattice scale, $g(a)^2$, decreases only as an inverse power of $\ln(a)$. This makes systematic improvement of perturbative results essentially impossible. This convergence may be improved when, following ideas from continuum perturbation theory [1], a renormalized or "boosted" [2] coupling rather than the bare coupling is used as an expansion parameter. Even so, considerable arbitrariness remains, and in general it is extremely difficult to go beyond one loop order in such calculations. To overcome these difficulties, Martinelli *et al.* [3] have proposed a promising nonperturbative renormalization procedure. This method has been previously used to determine renormalization coefficients for various operators using the Wilson [4–7] and staggered actions [8]. The purpose of this work is to study the application of this technique to the renormalization of the quark field and flavor nonsinglet fermion bilinear operators for the domain wall fermion action.

Domain wall fermions [9–11] provide an action, that at the expense of introducing a fifth dimension, has a low energy theory with excellent chiral properties while at the same time preserving exact flavor symmetry. These good chiral properties lead to a suppression of the possible dimension-5 terms in the long-distance effective Lagrangian implying that domain wall fermions define a lattice version of QCD which is off-shell improved to $\mathcal{O}(a^2)$. As we will see, these domain wall off-shell Green's functions show remarkably reduced lattice artifacts. A study of operator renormalization coefficients for this action is useful, both because these numbers are needed for use in practical calculations of physical quantities [12] and because it provides an excellent test of the chiral properties of the domain wall fermion action in practical simulations. In fact, we find that domain wall fermions perform quite well for nonperturbative renormalization with negligible contributions from explicit chiral symmetry breaking. This finding is in good agreement with recent work on the chiral limit of quenched QCD with domain wall fermions [12,13].

Careful operator normalization is especially important for the domain wall fermion method. As is reviewed in Sec. III A, the interpolating field conventionally used to create and destroy the physical modes is exactly localized in the fifth-dimension on the right and left walls. Since the actual physical modes extend somewhat into the fifth dimension, the overlap between the interpolating field and the physical modes will be smaller than 1. This implies a wave function renormalization factor (Z_q) which differs from one even in the case of free fields. For the eigenvectors corresponding to the smallest 19 Dirac eigenvalues examined in the quenched, $\beta = 6.0$ calculation of Ref. [12], this overlap typically varies between 75% and 85%. Fortunately, the nonperturbative methods employed here [3] precisely include these effects.

We begin in Sec. II with a brief summary of the main issues involved in applying the nonperturbative renormalization method. In Sec. III, we give the domain wall fermion action and discuss the Ward-Takahashi identities it obeys. Section IV builds on this base to constrain the ways in which explicit chiral symmetry breaking terms may enter low en-

---

*Present address: Department of Physics, Ohio State University, Columbus, OH 43210.

ergy matrix elements calculated using domain wall fermions. In Sec. V we give the details of our lattice simulations. Section VI describes the renormalization of the quark propagator, and in Sec. VII we introduce the quark bilinears and compute their renormalization on the lattice in the regularization independent scheme. After removing expected nonperturbative pole terms, we look for effects of explicit chiral symmetry breaking and find that they are negligible. In Sec. VIII, we avail ourselves of the axial Ward-Takahashi identity again to compute the quark wave function renormalization from the conserved vector and partially conserved axial-vector currents. In Sec. IX we calculate the renormalization of the nonconserved, local axial current from a ratio of its hadronic matrix element to the hadronic matrix element of the partially conserved axial current and find good agreement with the results of Sec. VII. In Sec. X we convert the renormalization coefficients to renormalization group invariant quantities by dividing out the renormalization group running. In Sec. XI we discuss the calculation of the quark wave function renormalization from the propagator.

After comparing our nonperturbative results with recent perturbative calculations in Sec. XII, we end with our conclusions. The details of the exact conventions and equations used for the perturbative running and matching are relegated to Appendixes.

II. NONPERTURBATIVE RENORMALIZATION

In the following the method of nonperturbative renormalization introduced in Ref. [3] will be studied. This method uses a renormalization scheme that is defined by a set of conditions that mandate the renormalized values of the operators of interest between external quark states, in a fixed gauge, at large virtualities. As such these conditions may be expressed in any regularization scheme [and so this scheme is known as the regularization independent (RI) scheme]. In particular this allows the renormalization factors to be defined in the lattice regularization, opening the way for renormalization factors to be directly calculated in numerical lattice simulations.

While calculating renormalization factors from lattice simulations neatly avoids the need to perform analytic calculations using lattice perturbation theory, which are both challenging and poorly behaved, doing so introduces several issues that must be considered.

Calculating the matrix elements of the operators of interest between external quark states requires a fixed gauge to be used. This allows for the appearance of Gribov copies, possibly obscuring the required comparison with continuum perturbation theory where only the trivial copy appears. Earlier studies [14] of the size of Gribov noise in the calculation of a gauge invariant normalization factor as a ratio of two gauge-variant amplitudes suggest this may not be an important difficulty for the parameters used here. However, in future work, this difficulty can be avoided by taking two steps: (i) Impose the regularization invariant normalization condition in a sufficiently small physical volume so that nonperturbative effects are suppressed. (ii) Begin the Landau gauge fixing procedure from a configuration that is in a com-

pletely fixed axial gauge. Taking these two precautions will insure that any effects of Gribov copies will be similar to other nonperturbative effects and will vanish as the comparison with perturbation theory is done at weaker and weaker coupling.

Numerical simulations are performed with a finite lattice spacing. This provides a natural condition,

$$|p| \ll \frac{1}{a}, \tag{1}$$

over the momenta range for which a direct extraction of continuum quantities is possible.

As the renormalization factors are determined in a nonperturbative calculation, the contributions of propagating mesons, and in particular pseudo-Goldstone bosons, must be identified and removed. These effects may be reduced by working at high momenta, with a natural condition for the absence of significant deviations being

$$\Lambda_{QCD} \ll |p|. \tag{2}$$

Taking the last two points together suggests that this technique relies on the existence of a "window" of momenta,

$$\Lambda_{QCD} \ll |p| \ll \frac{1}{a}, \tag{3}$$

for which the predictions of continuum perturbation theory should correctly describe the form of the lattice data. In practical simulations however, it has been found that the effects of deviations due to the violations of both these inequalities must be taken into account [4,15,7].

Fortunately, near either edge of this window, the form of deviations from perturbative behavior may be predicted. In the case of too low momenta, the initial corrections may be described by an expansion in terms of momentum-suppressed condensate terms by use of the operator product expansion (OPE). In turn, the first corrections to continuum-like behavior may be taken into account in terms of an expansion in the lattice spacing, a.

Another trivial consequence of the restricted range of momenta available in current lattice simulations is the need for many phenomenological calculations to be composed of continuum perturbation theory calculations at high scales, that are then run down to scales accessible on the lattice and combined with the lattice result. As the majority of the existing calculations for the continuum perturbative results use renormalization schemes that may only be defined when using dimensional regularization [such as the modified minimal subtraction ($\overline{\text{MS}}$) scheme], perturbative matching calculations between these schemes and the ones that may be defined in the lattice regularization need to be performed.

III. DOMAIN WALL FERMIONS

In this section the domain wall fermion formulation, as used in our simulations, will be reviewed.

A. Action

The domain wall fermion (DWF) method is a promising new approach to lattice QCD introduced in Ref. [10], which, at the expense of introducing an extra, discrete, non-gauge dimension, provides drastically improved chiral properties at finite lattice spacing while preserving exact symmetry under vectorial flavor rotations. This is achieved by using an action in the fifth dimension that is asymmetric between the left-handed and right-handed components of the fermion field. Denoting the fifth coordinate as s, with

$$s \in 0, \ldots, L_s - 1, \tag{4}$$

the massless action may be written as

$$S_{\text{fermion}}(m_f = 0) = -\sum_{x,s} \bar{\Psi}_{x,s} \left\{ -\gamma_\mu \frac{1}{2} (\nabla_\mu^+ + \nabla_\mu^-) \right.$$
$$+ \left[\frac{1}{2} \nabla_\mu^- \nabla_\mu^+ + M_5 \right]$$
$$\left. + P_L \partial_5^+ - P_R \partial_5^- \right\} \Psi_{x,s}, \tag{5}$$

with

$$Z = \int [dU][d\bar{\Psi} d\Psi] \exp(-S_{\text{gauge}} - S_{\text{fermion}}). \tag{6}$$

In Eqs. (5) and (6), $\Psi_{x,s}$ is the fermionic field, $U_\mu(x)$ is the gauge field and

$$S_{\text{gauge}} = \beta \sum_P \left(1 - \frac{1}{3} \text{Re Tr}[U_P] \right), \tag{7}$$

with $\beta = 6/g_0^2$ and g_0 is the bare lattice coupling. The projectors for the left and right-handed spinors are defined as

$$P_L = \frac{1}{2}(1 - \gamma^5)$$
$$P_R = \frac{1}{2}(1 + \gamma^5). \tag{8}$$

The notation $\nabla_\mu^\pm$ has been used to denote the discrete forward or backward covariant derivatives:

$$\nabla_\mu^+ \psi_x = [U_\mu(x)\psi_{x+\mu} - \psi_x] \tag{9}$$

$$\nabla_\mu^- \psi_x = [\psi_x - U_\mu^\dagger(x-\mu)\psi_{x-\mu}], \tag{10}$$

and $\partial_\mu^\pm$ represents the corresponding derivative with no gauge term. For the case of the derivative in the fifth dimension, $\partial_5^\pm$, the domain wall is implemented by giving the derivative hard boundaries. For example a one-dimensional ∂_5^+ acting on a space with four points may be written in matrix form as

$$\partial_5^+ \begin{pmatrix} \Psi_{x,0} \\ \Psi_{x,1} \\ \Psi_{x,2} \\ \Psi_{x,3} \end{pmatrix} = \begin{pmatrix} -1 & 1 & 0 & 0 \\ 0 & -1 & 1 & 0 \\ 0 & 0 & -1 & 1 \\ 0 & 0 & 0 & -1 \end{pmatrix} \begin{pmatrix} \Psi_{x,0} \\ \Psi_{x,1} \\ \Psi_{x,2} \\ \Psi_{x,3} \end{pmatrix}. \tag{11}$$

It should be noted that the action in Eq. (5) is actually the Hermitian conjugate of the action proposed in Ref. [10]. This change was made for practical reasons related to compatibility with the existing Wilson operator implementation for the QCDSP machine.

In the free theory, for $0 < M_5 < 2$, the effect of this is to produce a spectrum with one light fermionic mode, with exact chiral symmetry in the $L_s \to \infty$ limit, and $16L_s - 1$ heavy modes. The wave function of this light mode has its right-handed component concentrated on the wall at $s = L_s - 1$ and its left-handed component on the wall at $s = 0$. This light fermion mode may be studied by introducing an interpolating operator of the form [16]

$$q_x = P_L \Psi_{x,0} + P_R \Psi_{x,L_s-1}$$
$$\bar{q}_x = \bar{\Psi}_{x,0} P_R + \bar{\Psi}_{x,L_s-1} P_L. \tag{12}$$

The above considerations also naturally lead to the introduction of an explicit mass term to the action of the form

$$S_{\text{fermion}}(m_f) = S_{\text{fermion}}(m_f = 0) + \sum_x m_f \bar{q} q, \tag{13}$$

where m_f is the bare quark mass. In the free case, this leads to a spectrum with one light fermion of mass

$$M_5(2 - M_5)[m_f + (1 - M_5)^{L_s}]. \tag{14}$$

Note that in the $L_s \to \infty$ limit this is proportional to m_f, while for finite L_s there remains a residual mass, m_{res}, that acts as an additive renormalization to m_f.

However, the properties of domain wall fermions in the presence of gauge fields is a much more difficult question. In particular while the form of the mass of the light mode is expected to be proportional to $m_f + m_{\text{res}}$, the dependence of m_{res} on L_s must be determined. Perturbative calculations [17–21] have shown that the existence of the light mode is stable to small perturbations and that this mode has all chiral symmetry breaking proportional to m_f as $L_s \to \infty$. These studies also highlight several issues that must be considered when undertaking numerical simulations:

(i) The dependence of m_{res} on L_s may no longer be of the simple exponential form shown in Eq. (14).

(ii) M_5 undergoes a strong additive renormalization. This is understandable, as the five dimensional problem has no approximate chiral symmetry to protect it.

Indeed, extensive numerical studies in the quenched approximation [12,13] have shown that the L_s dependence of m_{res} does not fit a single exponential in the range $L_s = 12 \to 48$ for lattices with the same lattice spacing ($a = 0.520 \text{ GeV}^{-1}$) as the results in this paper. For $L_s = 16$, the

value used in this work, m_{res} was found to be ~ 4 MeV in the $\overline{\mathrm{MS}}$ scheme at 2 GeV [12]. The strong additive renormalization of M_5 requires that an input value be chosen numerically so that a single light mode forms and that its decay in L_s is as rapid as possible. It has been found that for even coarser lattices than used here such a choice can be made [22,12].

B. Lattice Ward-Takahashi identities

For the purpose of analyzing the consequences of the symmetries of the action, it is convenient to introduce an extended mass term, M, with flavor structure such that the mass term reads

$$\bar{q}_L M^\dagger q_R + \bar{q}_R M q_L, \tag{15}$$

and so the mass term is invariant under a transformation of the quark fields and the mass matrix M of the form

$$q_L \rightarrow U_L q_L$$

$$q_R \rightarrow U_R q_R \tag{16}$$

$$M \rightarrow U_R M U_L^\dagger.$$

Following Ref. [16], on a finite lattice, an exact vector Ward-Takahashi identity may be derived by considering transformations of the 5-dimensional fermion field, Ψ, such that

$$\delta_V \Psi_{x,s} = i\epsilon_x^a T^a \Psi_{x,s}$$
$$\delta_V \bar{\Psi}_{x,s} = -i\epsilon_x^a \bar{\Psi}_{x,s} T^a, \tag{17}$$

where $\{T^a\}$ is the set of Hermitian traceless matrices acting on $SU(N_f)$ flavor-space. This leads to an exact Ward-Takahashi identity that reads

$$-\partial_\mu^- \langle \mathcal{V}_\mu^a(z) O(x_1, \ldots, x_n) \rangle$$
$$+ \langle \bar{q}[M,T^a]q(z) O(x_1, \ldots, x_n) \rangle$$
$$= -i\langle \delta^a O(x_1, \ldots, x_n) \rangle, \tag{18}$$

where

$$\mathcal{V}_\mu^a(x) = \frac{1}{2} \sum_s [\bar{\Psi}_{x+\mu,s}(1+\gamma_\mu)U_{x,\mu}^\dagger T^a \Psi_{x,s}$$
$$- \bar{\Psi}_{x,s}(1-\gamma_\mu)U_{x,\mu}T^a\Psi_{x+\mu,s}]. \tag{19}$$

For the case of axial transformations the analogous choice is a transformation of the form

$$\delta_A \Psi_{x,s} = i\epsilon_{x,s}^a T^a \Psi_{x,s}$$
$$\delta_A \bar{\Psi}_{x,s} = -i\epsilon_{x,s}^a \bar{\Psi}_{x,s} T^a, \tag{20}$$

with

$$\epsilon_{x,s}^a = \begin{cases} \epsilon_x^a, & 0 \leq s < L_s/2 \\ -\epsilon_x^a, & L_s/2 \leq s < L_s. \end{cases} \tag{21}$$

This leads to a Ward-Takahashi identity of the form

$$-\partial_\mu^- \langle \mathcal{A}_\mu^a(z) O(x_1, \ldots, x_n) \rangle$$
$$+ \langle \bar{q}\{M,T^a\}\gamma_5 q(z) O(x_1, \ldots, x_n) \rangle$$
$$+ 2\langle J_{5q}^a O(x_1, \ldots, x_n) \rangle$$
$$= -i\langle \delta_A^a O(x_1, \ldots, x_n) \rangle, \tag{22}$$

where

$$\mathcal{A}_\mu^a = \frac{1}{2} \sum_s \mathrm{sgn}\left(s - \frac{L_s-1}{2}\right)$$
$$\times [\bar{\Psi}_{x+\mu,s}(1+\gamma_\mu)U_{x,\mu}^\dagger T^a \Psi_{x,s}$$
$$- \bar{\Psi}_{x,s}(1-\gamma_\mu)U_{x,\mu}T^a\Psi_{x+\mu,s}] \tag{23}$$

$$J_{5q}^a = -\bar{\Psi}_{x,L_s/2-1}P_L T^a \Psi_{x,L_s/2}$$
$$+ \bar{\Psi}_{x,L_s/2}P_R T^a \Psi_{x,L_s/2-1}. \tag{24}$$

Therefore, in contrast to the previous case, the axial current is not exactly conserved. This is necessary both to provide a mechanism for physical terms due to the $U(1)_A$ axial anomaly to enter the calculated amplitudes and also to allow for explicit chiral symmetry breaking contributions at finite L_s. The situation is analogous to that for Wilson fermions [23], where the role of J_{5q}^a is played by the chiral variation of the Wilson term, except that the contributions from J_{5q}^a are expected to tend to zero as $L_s \rightarrow \infty$ in the present case [16]. The form of the contributions from J_{5q}^a will be further discussed in the next section.

IV. OPERATOR MIXING AND CHIRAL SYMMETRY

The major attraction of the domain wall fermion formalism is its ability to decrease the size of chiral symmetry breaking by increasing the parameter L_s, the distance between the two four-dimensional lattice boundaries to which the left and right chiral modes are bound. However, it is often impractical or inefficient to choose such a large value of L_s that all chiral symmetry breaking effects from mixing between these walls can be neglected. Thus, it is important to characterize the effects of this chiral symmetry breaking and in this section we will determine how it can affect the low energy physics of lattice QCD. As we will see, this can be done as either an expansion in the size of the wall-mixing effects, which for simplicity we will denote by $\mathcal{O}(e^{-\alpha L_s})$ although the exact L_s dependence may be different, and/or as an expansion in the lattice spacing a.

This analysis is easily made by starting with the interpretation of chiral symmetry proposed by Furman and Shamir [16]. Here one identifies the full $SU(N_f)_L \otimes SU(N_f)_R$ chiral symmetry of the continuum theory as the independent

$SU(N_f)$ rotation of the fermion fields defined on the left- and right-hand halves of the five-dimensional lattice:

$$\Psi(x,s) \to U_L \Psi(x,s), \quad 0 \leq s \leq L_s/2 - 1$$
$$\Psi(x,s) \to U_R \Psi(x,s), \quad L_s/2 \leq s \leq L_s - 1, \qquad (25)$$

where U_L and U_R are $N_f \times N_f$ special unitary matrices belonging to the left and right factors of $SU(N_f)_L \otimes SU(N_f)_R$. From Eq. (12) it is clear that this transformation will act on the four-dimensional quark fields as a standard element of the full chiral symmetry.

Of course, the transformation in Eq. (25), whose generators are given in Eq. (20) and Eq. (17), cannot be an exact symmetry of the five-dimensional theory as the derivative terms in the fifth dimension, taken collectively, couple the left and right hand walls and prevent such independent rotations of this single, five-dimensional field. However, in the low energy sector of the theory this symmetry can be quite good. The physical, chiral modes which survive at low energy are expected to be exponentially bound to the walls with an overlap that is suppressed as L_s increases. The higher energy modes which can propagate freely between the walls are all far off-shell with propagators which are necessarily also exponentially suppressed at long distances, especially for the large distance L_s.

In order to characterize the effects of this controlled symmetry breaking that comes from communication between the walls, we will generalize somewhat the Dirac domain wall fermion operator of Shamir given in Eq. (13). We will introduce a special-unitary, flavor matrix Ω in the derivative term joining the four-dimensional planes $s = L_s/2 - 1$ and $s = L_s/2$. Thus, we will modify Eq. (5) by adding the term

$$S_\Omega = -\sum_x \{\bar{\Psi}_{x,L_s/2-1} P_L (\Omega^\dagger - 1) \Psi_{x,L_s/2}$$
$$+ \bar{\Psi}_{x,L_s/2} P_R (\Omega - 1) \Psi_{x,L_s/2-1}\}. \qquad (26)$$

If we include the transformation of the matrix Ω,

$$\Omega \to U_R \Omega U_L^\dagger, \qquad (27)$$

this generalized domain wall Dirac operator will now possess exact chiral symmetry. Note, a comparison with Eq. (16) shows that Ω transforms "like a mass term."

Thus, if we examine this generalized theory that includes the chiral matrix Ω, all amplitudes will become functions of Ω but will exactly obey the chiral symmetry described by Eq. (25) and Eq. (27). Therefore, we need only understand how the matrix Ω will enter the low energy Green's functions of interest to determine in a precise way the transformation properties of the chiral symmetry breaking induced by mixing between the walls.

To zeroth order in $e^{-\alpha L_s}$, the fermion degrees of freedom will remain bound to the walls and propagation from one wall to the other can be neglected. In such circumstances, the matrix Ω which is introduced at a point mid-way between the walls cannot enter, the amplitude will be independent of Ω and hence naively invariant under the full $SU(N_f)_L$ $\otimes SU(N_f)_R$ chiral symmetry. To the next order, $\propto e^{-\alpha L_s}$, we expect phenomena which involve a single propagation between $s = 0$ and $s = L_s - 1$. Thus, the matrix Ω should enter linearly in such amplitudes.

An important application of this analysis is to constrain the form of the effective continuum action which gives amplitudes that agree with those of the domain wall theory through a given order in the lattice spacing. To leading order in the lattice spacing, this effective Lagrangian has the standard continuum form. The above analysis requires that the mass term in this leading order effective Lagrangian must have the form

$$Z_m m_f \bar{\psi}\psi + c\{\bar{\psi}\Omega^\dagger P_R \psi + \bar{\psi}\Omega P_L \psi\}, \qquad (28)$$

where c is a constant with the dimensions of mass. Here the field ψ represents a conventional continuum multiplet of quark fields and all quantities carry their physical dimensions. The first piece is the normal chiral symmetry breaking introduced by the input mass m_f. The second comes from mixing between the walls and is required by the extended symmetry of Eq. (25) and Eq. (27) to be linear in Ω. Thus, this induced mass term can occur to first order in the mixing between the walls, permitting $c \propto e^{-\alpha L_s}/a$. With the conventional choice of Shamir, $\Omega_{a,b} = \delta_{a,b}$, the second term in Eq. (28) reduces to our usual residual mass term with $am_{\text{res}} \approx 10^{-3}$ [12].

In a similar fashion the $\mathcal{O}(a)$ effective Lagrangian will contain a clover term induced by mixing between the walls, again to first order in $e^{-\alpha L_s}$, since it also has the permitted $SU(N_f)_L \otimes SU(N_f)_R$ chiral structure:

$$ac_1\{\bar{\psi}\sigma_{\mu\nu}F_{\mu\nu}\Omega^\dagger P_R \psi + \bar{\psi}\sigma_{\mu\nu}F_{\mu\nu}\Omega P_L \psi\}, \qquad (29)$$

where $c_1 \propto e^{-\alpha L_s}$ is $\mathcal{O}(am_{\text{res}})$. Thus, such a term is suppressed both by the lattice spacing and by the smallness of m_{res}.

If we extend these considerations to $\mathcal{O}(a^2)$ terms in the effective Lagrangian, we can conclude that a four-Fermi operator of the form

$$c_2 a^2 (\bar{\psi}\psi)(\bar{\psi}\psi), \qquad (30)$$

where c_2 is a constant, cannot occur to order $e^{-\alpha L_s}$. Since this operator will become a chiral singlet only when contracted with two powers of the matrix Ω or one power of Ω and one power of the mass matrix M of Eq. (15), the coefficient of such an operator must contain a double suppression $c_2 \propto e^{-2\alpha L_s}$ or a further factor of m_f.

V. SIMULATION DETAILS

In the following discussions much use will be made of the momentum space quark propagator in Landau gauge. The first step in calculating this quantity is to fix the gauge. We implement Landau gauge fixing by iteratively sweeping over all lattice sites, maximizing the functional

$$\sum_{x,\mu} \{\text{Tr}[U_\mu(x) + U_\mu^\dagger(x)]\}. \qquad (31)$$

At each lattice site we determine a gauge transformation matrix, $g(x)$, which increases the value of Eq. (31). The maximum is achieved when

$$\sum_x \text{Tr}[B(x)B^\dagger(x)] \tag{32}$$

is zero, where

$$B(x) = A(x) - A^\dagger(x) - \frac{1}{3}\text{Tr}(A - A^\dagger) \tag{33}$$

$$A(x) = \sum_\mu \left[\tilde{U}_\mu^\dagger(x) + \tilde{U}_\mu(x - \mu)\right] \tag{34}$$

and

$$\tilde{U}_\mu(x) = g(x)U_\mu(x)g^\dagger(x + \mu). \tag{35}$$

In practice we stop when the quantity in Eq. (32) is smaller than 10^{-8}.

On this gauge-fixed configuration the quark propagator, $S(x,0)$, from one source, denoted as 0, to all possible sinks is then calculated. A discrete Fourier transform is then performed over the sink positions giving,

$$S(p,0) = \sum_x \exp(-ip^{\text{latt}} \cdot x)S(x,0), \tag{36}$$

with

$$p_\mu^{\text{latt}} = \frac{2\pi}{L_\mu}n_\mu, \tag{37}$$

where μ is one of x,y,z or t and n_μ may in principle lie in the range $0 \rightarrow L_\mu - 1$. In practice, however, only a subset of this range is used.

Unless otherwise stated all the data that will be presented are from calculations on a $16^3 \times 32 \times 16$ lattice (where the last number refers to the extent of the lattice in the fifth dimension). The simulation was performed at $\beta = 6.0$ with 2000 heatbath sweeps between every configuration and with 2000 thermalization sweeps performed at the outset. In total 142 configurations were generated. For this lattice size the momentum range was restricted to those momenta for which $n_\mu = 0,1,2$ for $\mu = x,y,z$ and $n_t = 0,1,2,3$. Quark propagators for 5 bare masses, $m_f = 0.01, 0.02, 0.03, 0.04$ and 0.05 were calculated all using $M_5 = 1.8$.

The results will often be quoted against the square of the absolute momentum, where this refers to the Euclidean inner product of the momentum defined in Eq. (37). To be more specific

$$(ap)^2 = \sum_\mu p_\mu^{\text{latt}} p_\mu^{\text{latt}}, \tag{38}$$

where p is dimensionful.

VI. THE RENORMALIZED PROPAGATOR

Before we treat the more complicated situation of the fermion bilinears it is necessary to first consider the renormalization of the quark propagator. Neglecting, for the moment, potential contributions from lattice artifacts the renormalized quark field may be defined as

$$q_{\text{ren}}(x) = Z_q^{1/2}q_0(x). \tag{39}$$

If we similarly introduce a renormalized mass, defined by

$$m_{\text{ren}} = Z_m m_0, \tag{40}$$

where m_0 represents a generic multiplicatively renormalized bare mass, then the renormalized propagator may be written

$$S_{\text{ren}}(p,m_{\text{ren}}) = Z_q S_0(p,m_0)\big|_{m_0 = m_{\text{ren}}/Z_m}. \tag{41}$$

Both Z_q and Z_m are fixed in the RI scheme by requiring that the renormalized propagator obey the Euclidean space relations

$$\lim_{m_{\text{ren}} \rightarrow 0} -\frac{i}{12}\text{Tr}\left(\frac{\partial S_{\text{ren}}^{-1}}{\partial \slashed{p}}(p)\right)_{p^2 = \mu^2} = 1 \tag{42}$$

$$\lim_{m_{\text{ren}} \rightarrow 0} \frac{1}{12m_{\text{ren}}}\text{Tr}(S_{\text{ren}}^{-1}(p))_{p^2 = \mu^2} = 1. \tag{43}$$

While Eq. (42) and Eq. (43) seem to give a simple and appealing way to calculate Z_q and Z_m by directly applying them to the lattice propagators, the effect of both lattice artifacts and spontaneous chiral symmetry breaking must be considered.

Lattice actions with explicit chiral symmetry breaking require an additive renormalization of the input mass, which may be taken into account for domain wall fermions by making the replacement

$$m_0 \rightarrow m_f + m_{\text{res}}, \tag{44}$$

in the equations above. However, the effects of lattice artifacts on the correct definition of the renormalized and improved quark field are more complicated. They have been studied in Ref. [24] for Wilson fermions, where it is noted that there are three terms that may mix with the definition at $\mathcal{O}(a)$ in the lattice spacing, giving rise to an expression for the improved and renormalized quark field of

$$q_{\text{ren}} = Z_q^{1/2}(1 + b_q ma)\{1 + ac_q'(\slashed{D} + m_{\text{ren}}) + ac_{\text{NGI}}\slashed{\partial}\}q_0, \tag{45}$$

where $\slashed{\partial}$ may appear because the gauge is fixed. If such extra terms appear then conditions must be found that allow them to be subtracted from the bare quark field before Eq. (42) and Eq. (43) may be applied. In the context of simulations using $\mathcal{O}(a)$ improved Wilson action at $\beta = 6.0$ these terms have been found to give significant contributions to the form of the propagator [24]. In particular c_q' was found to be large. However, they all break chiral symmetry and so, following
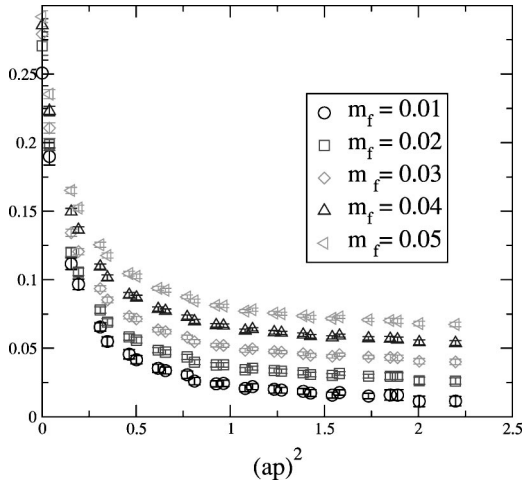
FIG. 1. A plot of $\frac{1}{12}\mathrm{Tr}(S_{latt}^{-1})$ versus $(ap)^2$ showing that for moderate values of $(ap)^2$ the effects of explicit chiral symmetry breaking are small.

the arguments of Sec. IV, should be suppressed by a factor of $O(am_{\mathrm{res}})$ for simulations using domain wall fermions. As such, studying the form of the propagator provides an excellent test of the chiral properties of domain wall fermions.

The effects of spontaneous chiral symmetry breaking on the form of the propagator are well known [25,26]. The most noticeable effect is that the trace of the inverse propagator picks up an extra contribution, which at lowest order in a power expansion in $1/p^2$ may be described as

$$\frac{1}{12}\mathrm{Tr}(S_{\mathrm{ren}}^{-1}(p)) = m_{\mathrm{ren}} + C_1 \frac{\langle \bar{q}q \rangle}{p^2} + \cdots \qquad (46)$$

where, at first order in perturbation theory, $C_1 = 4\pi\alpha_s/3$. Putting Eq. (46) and Eq. (45) together, the predicted form for the trace of the lattice quark propagator is

$$\frac{1}{12}\mathrm{Tr}(S_{\mathrm{latt}}^{-1}(ap)) = \cdots + \frac{a^3\langle \bar{q}q \rangle}{(ap)^2}C_1 Z_q + Z_m Z_q\{am_f + am_{\mathrm{res}}\}$$
$$+ 2(c_{\mathrm{NGI}}Z_q - c_q')(ap)^2 + \cdots, \qquad (47)$$

where terms of $\mathcal{O}(mc_{\mathrm{NGI}})$ have been neglected.

In Fig. 1 we plot the left-hand side of Eq. (47) versus $(ap)^2$ for a variety of values for m_f. As can be seen, for domain wall fermions this quantity approaches a constant value for moderately large values of $(ap)^2$. Also, it is encouraging that while at low momenta the effects of spontaneous chiral symmetry are visible, there is no evidence to suggest appreciable effects from explicit chiral symmetry breaking. In particular, there is no evidence of a large additive mass renormalization. This is visible in Fig. 2, which shows the result of a linear extrapolation of the data to the point $m_f = 0$. Figure 3 shows the slope of this extrapolation, which from Eq. (47) is $Z_m Z_q$ at large $(ap)^2$.
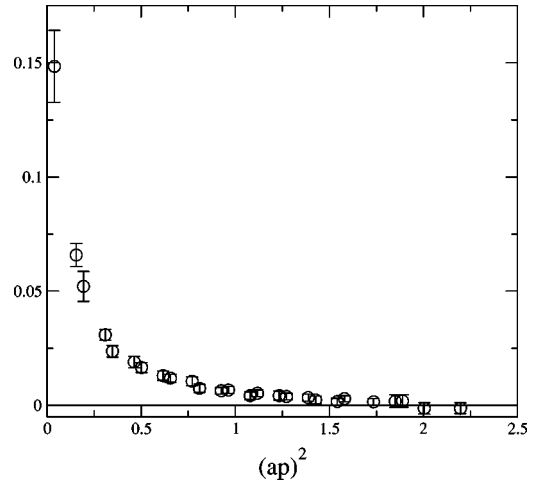

FIG. 2. The value of $\frac{1}{12}\mathrm{Tr}(S^{-1})$ extrapolated to $m_f = 0$ vs $(ap)^2$. For moderate $(ap)^2$ the extrapolated value is zero within errors, showing that the residual mass is small.

A. Extracting Z_q from the propagator

The extraction of Z_q from the propagator via Eq. (42) is numerically challenging due to the need for a discrete derivative to be calculated. A much simpler method [3], is to calculate

$$Z_q' = -i\frac{1}{12}\sum_\mu \frac{ap_\mu}{(ap)^2}\mathrm{Tr}(\gamma_\mu S_{\mathrm{latt}}^{-1}(ap)). \qquad (48)$$

This quantity may then be related to Z_q by a perturbative matching calculation performed in the continuum [27].

On the other hand, the use of Z_q' to determine Z_q introduces significant $O(a^2)$ errors through the choice of how the discretized momenta are defined. If we were to replace in Eq. (48) the definition of the lattice momentum in Eq. (37) by, for example,
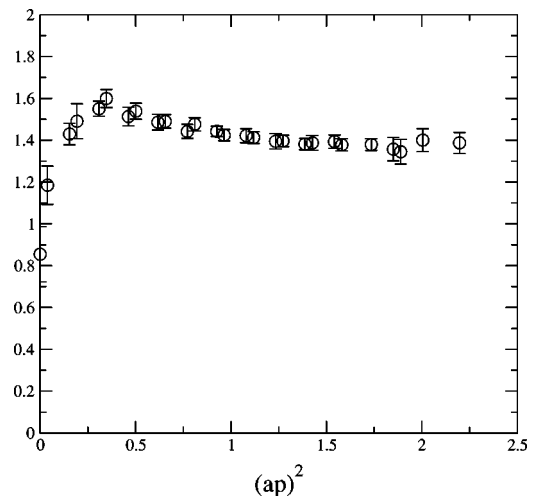
$$\bar{p}_\mu = \frac{1}{a}\sin p_\mu a, \qquad (49)$$

FIG. 3. $Z_m Z_q$ calculated from the slope of $\frac{1}{12}\mathrm{Tr}(S^{-1})$ versus m_f plotted as a function of $(ap)^2$.

then the resulting Z'_q would differ from that given in Eq. (48) by $O(a^2)$ because the trace includes an explicit factor of $p_\mu \gamma_\mu$. One can estimate the size of this error by using various definitions for the lattice momentum in the analysis. As will be shown later in Sec. XI, this uncertainty is roughly 10–20 %. In Secs. VIII and IX we introduce two methods for computing Z_q which avoid this uncertainty.

VII. FLAVOR NONSINGLET FERMION BILINEARS

A. Introduction

In the following the renormalization of the flavor non-singlet fermion bilinear operators will be considered. To simplify notation explicit quark flavors (u and d) will be used in the following equations. The most general fermion bilinear may be written as $\bar{u}\Gamma_i d$ with

$$\Gamma_i \in \{1, \gamma_\mu, \gamma_5, \gamma_\mu \gamma_5, \sigma_{\mu\nu}\}, \tag{50}$$

where i represents whatever indices the gamma matrices have. The renormalized operator is defined as

$$[\bar{u}\Gamma d]_{\text{ren}} = Z_\Gamma [\bar{u}\Gamma d]_0. \tag{51}$$

The factor Z_Γ is fixed in the RI scheme by defining the unrenormalized, amputated vertex function

$$\Pi_{\Gamma,0}(p,q) = \frac{1}{V} \int d^4z \, d^4x_1 d^4x_2 e^{-ip \cdot x_1 + iq \cdot x_2}$$

$$\times \langle [\bar{u}\Gamma d]_0(z) u_0(x_1) \overline{d_0}(x_2) \rangle_{\text{AMP}}, \tag{52}$$

the corresponding renormalized, amputated vertex function

$$\Pi_{\Gamma,\text{ren}}(p,q) = \frac{Z_\Gamma}{Z_q} \Pi_{\Gamma,0}(p,q) \tag{53}$$

and requiring that

$$\Lambda_{\Gamma_i,\text{ren}}(p,p)_{p^2=\mu^2}$$

$$= \frac{1}{\text{Tr}\left(\sum_i \Gamma_i \Gamma_i\right)} \text{Tr}\left(\sum_i \Gamma_i \Pi_{\Gamma_i,\text{ren}}(p,p)\right)_{p^2=\mu^2} = 1. \tag{54}$$

Note, the corresponding, unrenormalized vertex amplitude is defined by

$$\Lambda_{\Gamma,0} = \frac{1}{\text{Tr}\left(\sum_i \Gamma_i \Gamma_i\right)} \text{Tr}\left(\sum_i \Gamma_i \Pi_{\Gamma_i,0}(p,p)\right), \tag{55}$$

so that

$$\Lambda_{\Gamma_i,\text{ren}}(p,p) = \frac{Z_\Gamma}{Z_q} \Lambda_{\Gamma_i,0}(p,p). \tag{56}$$

While Eq. (56) completely defines a procedure for calculating a renormalization factor for the bilinear operator of interest, practically we need to be able to use a renormalization condition that allows us to match to perturbative calculations. In general the value of $\Lambda_{\Gamma_i,0}(p,p)$ has contributions from intrinsically non-perturbative effects (such as those due to propagating pions) that perturbative calculations do not include. As we are interested in the value of the renormalization factors in the perturbative regime we either apply the renormalization condition at a high enough momenta such that the nonperturbative effects are suppressed, or remove such effects from the data and in the following that is what we will do. We will reserve the notation Z_i, $i \in \{q, S, P, T, A, V\}$ for the renormalization factors in the perturbative regime.

B. Z_A and Z_V

A (partially) conserved current that is normalized in a fashion which is consistent with the usual Ward-Takahashi identities will undergo no renormalization and the corresponding Z_Γ will be unity. In particular, for domain wall fermions and the RI renormalization scheme specified by Eqs. (42) and (54) and imposed at high-momentum, $\mu \gg \Lambda_{QCD}$, we expect

$$Z_\mathcal{A} = Z_\mathcal{V} = 1. \tag{57}$$

However, on the lattice the (partially) conserved currents are not local and it is frequently more convenient to work with their local counterparts. Provided that these are related by a chiral transformation one still has

$$Z_A = Z_V. \tag{58}$$

This does not, however, mean that Λ_A must equal Λ_V, and several mechanisms exist for splitting them away from each other at low energies.

Even if there are no significant effects from explicit chiral symmetry breaking, the effects of spontaneous chiral symmetry breaking must be taken into account. Consideration of the operator product expansion, to lowest order in powers of $1/p^2$, shows that Λ_A and Λ_V may get contributions from terms of the form

$$\frac{m_{\text{ren}}^2}{p^2} \tag{59}$$

and

$$\frac{m_{\text{ren}} \langle \bar{q}q \rangle}{p^4}. \tag{60}$$

Since such terms, by their very nature, stem from chiral symmetry breaking they are not constrained to enter Λ_A and Λ_V with the same weight. At large momenta these terms are suppressed and do not affect the extraction of Z_A and Z_V.

If the action being used explicitly breaks chiral symmetry, Z_A and Z_V need not be equal, but their ratio will still be scale
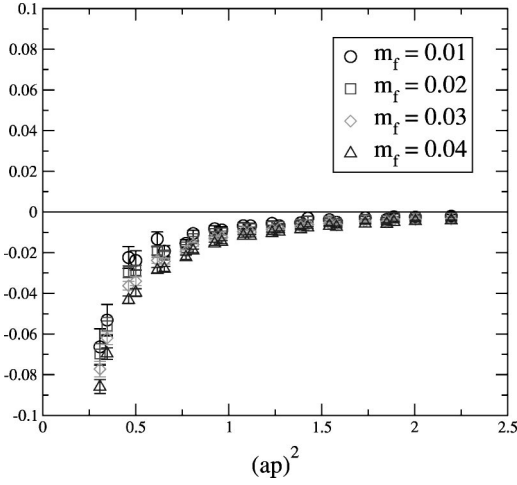
FIG. 4. A plot of $\Lambda_A - \Lambda_V$ versus $(ap)^2$, showing that there is no significant difference between Z_A and Z_V, even for moderate values of $(ap)^2$.

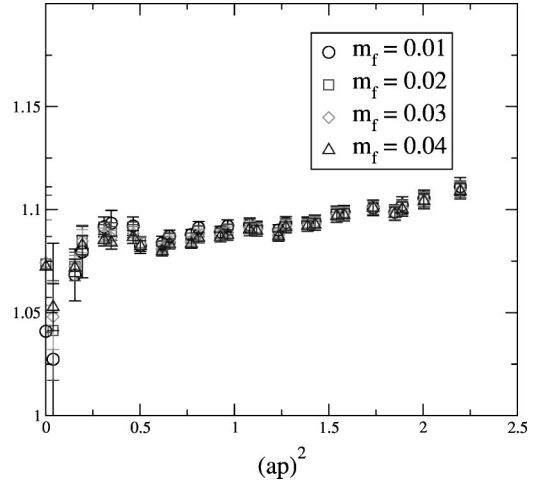

FIG. 5. A graph of $\frac{1}{2}\{\Lambda_A + \Lambda_V\}$ versus $(ap)^2$, which up to lattice artifacts, gives Z_A/Z_q and Z_V/Z_q.

independent. This means that while Λ_A and Λ_V need not approach one another at high momenta, their ratio should become scale independent for large enough momenta.

While we want to work in the chiral limit for the extraction of the renormalization factors it is also worthwhile to consider what the mass dependence of Λ_A and Λ_V should be (especially as we wish to extract the chiral limit from data measured in finite mass simulations). Requiring that the "generalized" symmetry introduced in Eq. (16) is satisfied constrains the mass dependence to either be of the same form as Eq. (59) (a single power of mass multiplying something that breaks chiral symmetry—and therefore by the argument of the previous paragraph damped with momentum) or proportional to a second or higher power of mass. In the latter case any effect on our data should be negligible.

The above considerations suggest looking at the quantity

$$\Lambda_A - \Lambda_V. \tag{61}$$

This is shown in Fig. 4 and, as with the case for the quark propagator, while the effects of nonperturbative breaking terms are visible at low momenta, they are damped at higher momenta. There is no significant signal for effects from explicit chiral symmetry breaking, since $\Lambda_A - \Lambda_V$ is tending to zero. At momenta of interest, there also seems to be no significant splitting due to nonperturbative effects with the difference between Λ_A and Λ_V being less than 1% in the chiral limit at $(ap)^2 = 0.8$ and smaller for momenta above this. This being so, it is sensible to use the quantity $\frac{1}{2}(\Lambda_A + \Lambda_V)$ for the extraction of both Z_A/Z_q and Z_V/Z_q to increase the statistical accuracy. This is shown in Fig. 5.

C. Z_S and Z_P

For a theory with chiral symmetry the RI scheme preserves the well known $\overline{MS}$ relations

$$Z_S = Z_P \tag{62}$$

$$Z_m = \frac{1}{Z_S}. \tag{63}$$

If the potential for explicit chiral symmetry breaking is taken into account, these equalities cease to be valid, but the quantities Z_S/Z_P, $Z_S Z_m$ and $Z_m Z_P$ are expected to be scale independent. However, lattice studies using both the Wilson and staggered actions have shown that the ratio Λ_P/Λ_S, which in perturbation theory would be equal to Z_S/Z_P and therefore might be expected to be momentum independent up to small corrections, is strongly momentum and mass dependent, with the bulk of this dependence arising from Λ_P. It is instructive to consider the source of this discrepancy [3,28]. We start from the continuum axial Ward-Takahashi identity which is derived by taking the axial variation of the quark propagator. This reads

$$(m_u + m_d) \int dz \langle u(x_1)[\bar{u}\gamma_5 d](z)\bar{d}(x_2)\rangle$$
$$= \gamma_5 \langle d(x_1)\bar{d}(x_2)\rangle + \langle u(x_1)\bar{u}(x_2)\rangle\gamma_5. \tag{64}$$

Moving to momentum space gives

$$(m_u + m_d)\langle u[\bar{u}\gamma_5 d]\bar{d}\rangle(p,p) = \gamma_5\langle d\bar{d}\rangle(p) + \langle u\bar{u}\rangle(p)\gamma_5, \tag{65}$$

which in the $m_u \to m_d \equiv m$ limit gives

$$2m\langle u[\bar{u}\gamma_5 d]\bar{d}\rangle(p,p) = \{\gamma_5, S(p)\}. \tag{66}$$

Amputating and tracing with γ_5 yields

$$m\Lambda_P(p,p) = \frac{1}{12}\mathrm{Tr}(S^{-1}(p)). \tag{67}$$

Neglecting all lattice artifact terms except the additive mass renormalization (which is justified by the discussions in Sec. VI), this leads to an approximate expression for $\Lambda_{P,\mathrm{latt}}$, including the first order contribution of spontaneous chiral symmetry breaking:
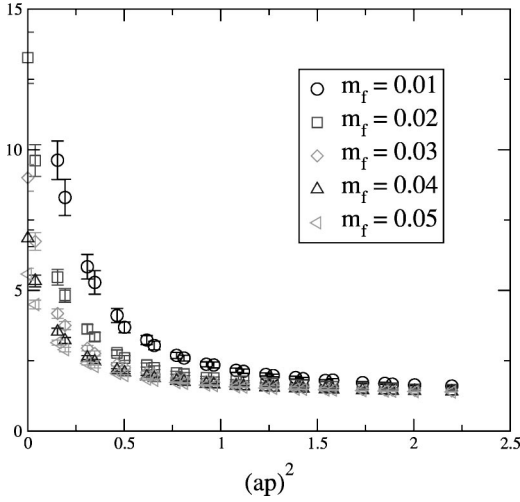
FIG. 6. Λ_P versus $(ap)^2$ for several values of m_f, showing that the $1/p^2$ pole is more pronounced for small m_f.

$$(m_f+m_{\text{res}})\Lambda_{P,\text{latt}}(ap,ap)=\cdots+\frac{a^2\langle\bar{q}q\rangle}{(ap)^2}C_1Z_q$$

$$+Z_mZ_q(m_f+m_{\text{res}}),\quad (68)$$

neglecting terms of $\mathcal{O}[(ap)^2]$. While in the absence of the condensate term this equation reduces to $Z_P=1/Z_m$, the condensate term, which is clearly visible in Fig. 2, gives rise to a pole term of the form

$$\frac{\langle\bar{q}q\rangle}{(m_f+m_{res})(ap)^2}C_1Z_q \quad (69)$$

in $\Lambda_{P,\text{latt}}$. Figure 6 shows the data for $\Lambda_{P,\text{latt}}$ with this effect clearly visible, with the rise for small $(ap)^2$ becoming much more pronounced as the mass decreases.

A similar argument may be put forward for Λ_S. In this case it is the Ward-Takahashi identity arising from a vector rotation of the fields:

$$(m_u-m_d)\int dz\langle u(x_1)[\bar{u}d](z)\bar{d}(x_2)\rangle$$

$$=\langle d(x_1)\bar{d}(x_2)\rangle-\langle u(x_1)\bar{u}(x_2)\rangle. \quad (70)$$

Moving to momentum space, this gives

$$(m_u-m_d)\langle u[\bar{u}d]\bar{d}\rangle(p,p)=\langle d\bar{d}\rangle(p)-\langle u\bar{u}\rangle(p), \quad (71)$$

which in the $m_u\to m_d$ limit tends to

$$\langle u[\bar{u}d]\bar{d}\rangle(p,p)=-\frac{\partial}{\partial m}S(p). \quad (72)$$

Finally, amputating and tracing gives

$$\Lambda_S=\frac{1}{12}\frac{\partial\,\text{Tr}[S(p)^{-1}]}{\partial m}. \quad (73)$$

Note that this relation should be exact for domain wall fermions (with $m=m_f$) for any value of L_s. Using Eq. (47), and noting that both the residual mass and the renormalization factors should be independent of m_f, gives the approximate expression

$$\Lambda_{S,\text{latt}}=Z_mZ_q+\frac{C_1Z_q}{(ap)^2}\frac{\partial a^3\langle\bar{q}q\rangle}{\partial(am_f)}. \quad (74)$$

If the mass dependence of $\langle\bar{q}q\rangle$, for small masses, is proportional to only positive powers of the mass, then the second term in Eq. (74) is almost certainly unimportant as it is suppressed in exactly the region of parameter space in which we are working: large momenta and small masses. (The effect might be larger than naively expected, as $\langle\bar{q}q\rangle$ is quadratically divergent in the lattice spacing.) It is necessary, however, to consider the effects of fermionic zero-modes on $\langle\bar{q}q\rangle$. Assuming a theory with chiral symmetry, the spectral decomposition of the quark propagator leads to an expected form for $\langle\bar{q}q\rangle$, on a single configuration C, of

$$-\langle\bar{q}q\rangle_C=\text{Tr}[(\slashed{D}+m)^{-1}] \quad (75)$$

$$=\frac{n_0}{mV}+\frac{1}{V}\sum_{\lambda_n>0}\frac{1}{m+i\lambda_n},\quad n_0\geq0, \quad (76)$$

where n_0 is the number of fermionic zero-modes, V is the four dimensional space-time volume and the λ_n are such that $\slashed{D}\psi_n=i\lambda_n\psi_n$. The number of such zero modes should grow more slowly than the volume, and so the first term in Eq. (76) will vanish in the infinite volume limit. However, for the lattice parameters used for this simulation the effects of zero-modes have been found to be noticeable in both $\langle\bar{q}q\rangle$ and hadronic spectrum calculations [12] and so must be considered for the present case. Comparing Eq. (74) and Eq. (76) shows that, as $m\to0$ for fixed momentum, Λ_S gets a large contribution from zero-modes of the form

$$-\frac{1}{m^2}\langle n_0\rangle\frac{C_1Z_q}{p^2}, \quad (77)$$

that must be subtracted before Z_S/Z_q may be calculated from Eq. (54). Figure 7 shows our data for $\Lambda_{S,\text{latt}}$. While the effect of the condensate term is smaller than that for Z_P, it is noticeable for the lighter masses.

D. Fitting the pole terms

Considering Eq. (77) and moving to lattice notation, the method for extracting Z_S from Λ_S becomes clear. Working at a fixed momentum, Λ_S may be fitted to the form

$$\Lambda_{S,\text{latt}}=\frac{c_{1,S}}{[am_f+\mathcal{O}(am_{\text{res}})]^2}+c_{2,S}+c_{3,S}(am_f)^2, \quad (78)$$

with Z_q/Z_S being given by $c_{2,S}$. While one might naively expect the denominator in the above equation to be am_f+am_{res}, as shown in Ref. [12] the residual chiral symmetry
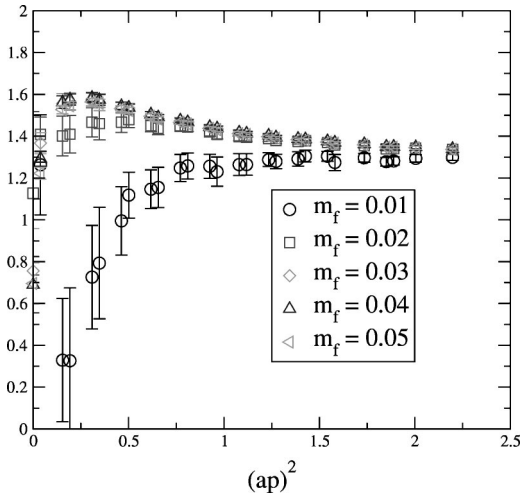
FIG. 7. A plot of $\Lambda_{S,\text{latt}}$ versus $(ap)^2$ for several masses. The mass pole can be clearly seen for small momenta and is attributable to zero-mode effects.

FIG. 8. This figure displays the average χ^2 per degree of freedom for the fits used to determine the power of the mass poles in Λ_S and Λ_P, clearly showing their $1/m^2$ and $1/m$ poles, respectively.

breaking effects that appear in the pole term in $\bar{q}q$ are not parametrized precisely by am_{res} since the singular behavior of the pole enhances what are expected to be order a^2 variations in the quantity am_{res}. One only knows that the residual chiral symmetry breaking effects are of $\mathcal{O}(am_{\text{res}})$. However, for the pole subtractions in this paper we have used precisely $am_f + am_{\text{res}}$. This is justified since the statistical errors on our data are such that the fits are insensitive to the exact value of m_{res}.

The situation for the Z_P extraction is slightly more complicated. Examining Eq. (68) and Eq. (76), shows that Λ_P should have a double pole of the form

$$\Lambda_{P,\text{latt}} = \frac{c_{1,P}}{(am_f + am_{\text{res}})^2} + \frac{c_{2,P}}{(am_f + am_{\text{res}})}$$
$$+ c_{3,P} + c_{4,P}(am_f)^2, \qquad (79)$$

with $c_{3,P}$ being equal to Z_q/Z_P and the quadratic mass pole due to zero-mode effects in $\langle \bar{q}q \rangle$. For simplicity, we have again used $am_f + am_{\text{res}}$ in the first term of the right-hand side in Eq. (79). For practical purposes, however, the need to fit to the quadratic term may be avoided by working with $m_f \geq 0.02$. Good evidence that the above fitting forms are correct is shown in Fig. 8. This shows the average, over all the momenta in the range $0.5 < (ap)^2 < 2.0$, of the χ^2 per degree of freedom for a correlated fit to the above forms for m_f dependence with the power of the pole treated as a free parameter. One sees that a $1/m$ pole is favored for the Z_P case while a $1/m^2$ is identified in the fit for Z_S. Further evidence is provided by considering the resulting values for Z_S/Z_q and Z_P/Z_q. Figure 9 shows a comparison between the extracted values of these two quantities. As chiral symmetry would predict for Z_S/Z_q and Z_P/Z_q, the two quantities coincide at large momenta. This provides an excellent test of both the extraction method and the chiral properties of domain wall fermions. This can be further seen by comparing
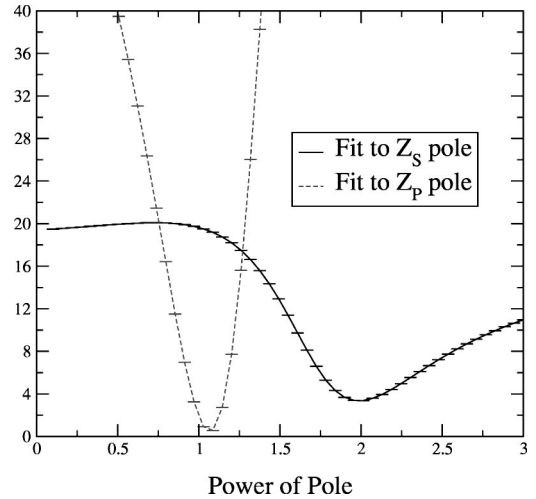
Z_P and Z_m (as calculated from the trace of the inverse propagator), which is shown in Fig. 10. This product is clearly very close to unity.

E. Z_T

The tensor density renormalization, while sometimes neglected in bilinear renormalization coefficient calculations, is a quantity of use to current lattice simulations [29]. An extraction of its value will be postponed to Sec. X, but for completeness a plot of Λ_T is shown in Fig. 11.

VIII. EXTRACTING Z_q FROM THE EXACT WARD IDENTITIES

The vector Ward-Takahashi identity of Eq. (18) is exact at finite lattice spacing. As such, the renormalization coefficient for the conserved vector current defined in Eq. (19), is equal to unity. Additionally, the considerations of Sec. IV show
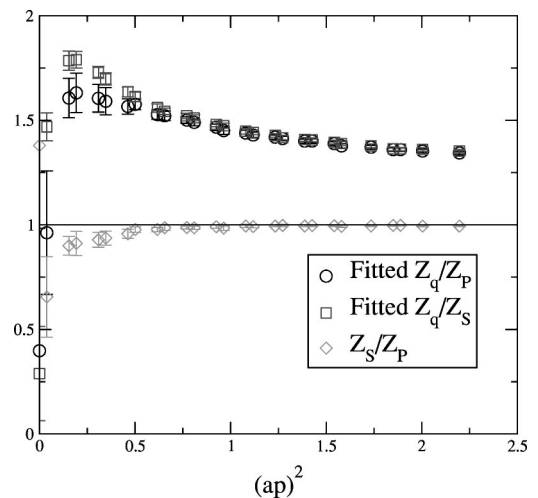

FIG. 9. A comparison of Z_S/Z_q and Z_P/Z_q as extracted from Λ_S and Λ_P after pole subtraction.
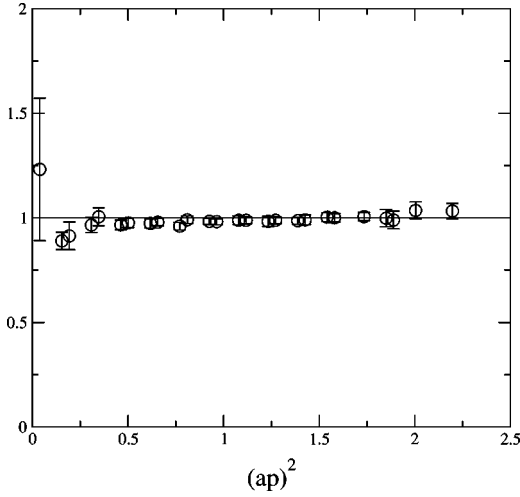
FIG. 10. The product $Z_P Z_m$ calculated by combining Z_P/Z_q from pole subtraction with the trace of the inverse propagator. This product is clearly unity within errors.

that through first order in the residual chiral symmetry breaking the extra J_{5q}^a in Eq. (22) can be completely absorbed into the additive renormalization of the mass so that the axial Ward-Takahashi identity, for low-energy physics, takes on the normal, continuum form. Therefore, the renormalization factor for the axial current defined by Eq. (23) should also be unity to a good approximation.

The above facts can be used to compute the quark field renormalization Z_q from Eq. (54), as applied the conserved vector and axial currents. For the case of the conserved vector current Eq. (54) reads

$$Z_q^{-1} Z_V \frac{1}{48} \mathrm{Tr}(\gamma^\mu \Lambda_V^\mu(p)) = 1 \tag{80}$$

which therefore implies

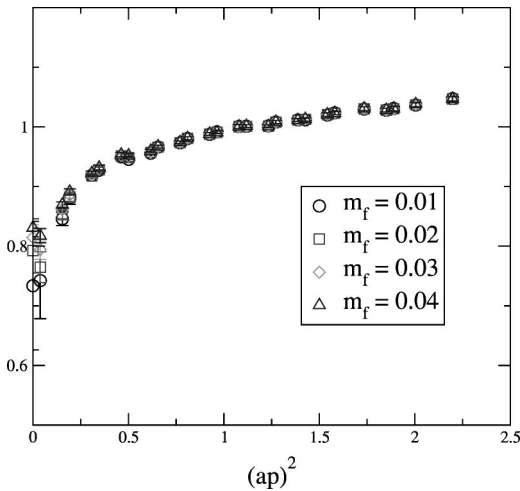$$Z_q = \frac{1}{48} \mathrm{Tr}(\gamma^\mu \Lambda_V^\mu(p)). \tag{81}$$

FIG. 11. This is a graph of Λ_T versus $(ap)^2$, from which Z_T will be extracted in Sec. X.

A similar equation also holds for the conserved axial current.

Because the formulas for the conserved currents contain fermion fields at separate points on the lattice as well as summation over all s, the calculation of the matrix elements for these operators can be very expensive. We used a random source estimator to compute the part of the sum between $s = 1$ to $s = L_s - 2$. Also, instead of calculating all four components of $\Lambda^\mu(p)$ for a given momentum p, we calculate $\Lambda^0(p)$ for momenta related to p by interchange of its 0th component with each of the other three. We then use the equality

$$\begin{aligned}
\mathrm{Tr}(\gamma^\mu \Lambda_V^\mu(p^0,p^1,p^2,p^3)) &= \mathrm{Tr}(\gamma^0 \Lambda_V^0(p^0,p^1,p^2,p^3)) \\
&\quad + \mathrm{Tr}(\gamma^0 \Lambda_V^0(p^1,p^0,p^2,p^3)) \\
&\quad + \mathrm{Tr}(\gamma^0 \Lambda_V^0(p^2,p^1,p^0,p^3)) \\
&\quad + \mathrm{Tr}(\gamma^0 \Lambda_V^0(p^3,p^1,p^2,p^0)),
\end{aligned} \tag{82}$$

to obtain the needed result. As the time to Fourier transform of a matrix element is negligible in comparison with the calculation of the matrix element itself, this allows us to obtain the result with only a quarter of the running time of direct calculation of Λ_V^μ.

Because the volume $16^3 \times 32$ used in the simulations is not symmetric, strictly speaking the above equation is not exact, as the third component of momentum is not related by symmetry to the first and second ones. However, this difference is suppressed by two powers of the lattice spacing and, in practice, the results obtained for the last three terms in Eq. (82) all agree within statistical errors for the momenta used. We used momenta with the first three integer components no larger than 2 and the last component equal to 0 or 2. The two exceptions were the momenta with integer components (2,2,2,0) and (2,2,2,2) that were excluded since they would require usage of momenta (0,2,2,4) and (1,2,2,4).

Figure 12 shows the difference between Z_q calculated using the axial and vector Ward-Takahashi identities, while Fig. 13 shows the average. As can be seen from Fig. 12, while for low momenta the two methods give different results, this difference is damped at large momenta as would be expected if this effect stems from spontaneous (rather than explicit) chiral symmetry breaking. Again, this provides strong evidence that the effects of explicit chiral symmetry breaking are negligible in these calculations.

IX. Z_A FROM HADRONIC MATRIX ELEMENTS

As mentioned in Sec. VIII, to a good approximation the axial current defined by Eq. (23) is conserved, and therefore has a renormalization coefficient equal to the identity. This provides a simple way to calculate the renormalization coefficient of the local axial current operator, Z_A, directly from hadronic matrix element calculations. One method, that has been used in Ref. [12], is to note that the matrix element of any operator with the renormalized axial current is a well defined quantity, which will be independent of the interpolating operator for the axial current at distances above the
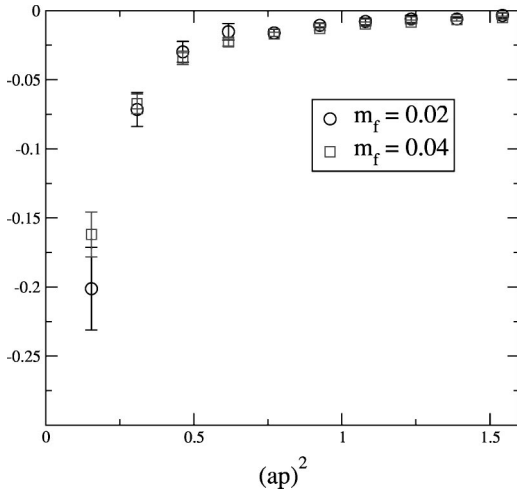
FIG. 12. The difference between Z_q as extracted from the conserved axial vector and vector currents.

scale of the lattice spacing. Therefore,

$$\langle \mathcal{A}_0(t_1)\bar{q}\gamma_5 q(t_2)\rangle = Z_A\langle A_0(t_1)\bar{q}\gamma_5 q(t_2)\rangle \qquad (83)$$

for $|t_1-t_2|a \gg 1$. A full discussion of this method and the results are given in Ref. [12], but it is useful to summarize the results here. Table I collects together values for Z_A for several L_S values on a $\beta=6.0$, $16^3 \times 32$ lattice with $M_5 = 1.8$. The quoted errors are statistical only.

X. RENORMALIZATION GROUP BEHAVIOR

The previous sections have provided an extraction of the renormalization coefficients of interest taking into account the possible effects stemming from chiral symmetry breaking (either explicit or spontaneous). In general, perturbation theory predicts that these coefficients may be logarithmically dependent on the momentum scale. Lattice artifacts may also cause the result to depend on the definition of momentum on the lattice. When small, these lattice artifacts will be manifest in the data as added terms proportional to $(ap)^2$.
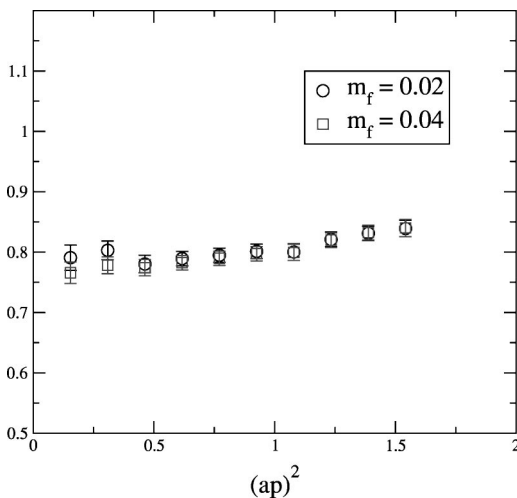

FIG. 13. The average of Z_q from the conserved axial vector and vector currents.

TABLE I. Z_A computed from the ratios of hadronic matrix elements.

L_S	Z_A	no. configs.
12	0.7560(3)	56
16	0.7555(3)	56
24	0.7542(3)	56
32	0.7535(3)	72
48	0.7533(3)	64

fest in the data as added terms proportional to $(ap)^2$.

The simplest approach to using the renormalization coefficients calculated in this paper is to take the (mass-pole subtracted) value for $\Lambda_i(ap)$ as $(Z_q/Z_i)(ap)$. However, we need to address two significant uncertainties.

First, this choice assumes, without verification, that the $\mathcal{O}[(ap)^2]$ lattice artifacts are small. We should attempt to understand the momentum dependence of the amplitude $\Lambda_i(ap)$ to determine the size of the $\mathcal{O}[(ap)^2]$ contamination and, if possible, remove it.

Second, most operators of interest in lattice calculations are ultimately defined using continuum perturbation theory. Making this connection requires the use of perturbation theory to connect the RI scheme and momentum scale used here with the renormalization procedure and momentum scale used in the original continuum definition, typically the $\overline{\text{MS}}$ scheme. This final matching step between the normalized lattice and continuum operators is done at a specific momentum scale for the renormalized lattice operator. In general, both the normalization of lattice operators and the matching coefficients will depend on this momentum scale. It is not known *a priori* how many loops in perturbation theory must be calculated to correctly describe the momentum range probed in current lattice calculations, or even if perturbation theory can describe the region we are studying. Comparing the momentum behavior predicted from perturbation theory to that of the data therefore provides an important consistency check for the general framework of the method.

Our approach to comparing the known perturbative running of the quantities of interest to our numerical data will be to divide the data by the predicted renormalization group running, with the overall normalization set by requiring that at the point $(ap)^2=1$ this divisor is one. If the perturbative result correctly describes the data, and the effect of $(ap)^2$ terms may be neglected, the result will be completely scale independent.

There are three components that are needed to calculate these quantities.

(i) The anomalous dimensions for the operators from perturbation theory.

(ii) The ratio of $Z^{\text{RI}}/Z^{\overline{\text{MS}}}$ must be known to perform the matching. Since the renormalization condition that determines Z^{RI} is well defined both on the lattice and in continuum dimensional regularization this ratio may be calculated perturbatively using the latter regularization. In general it can be expanded as
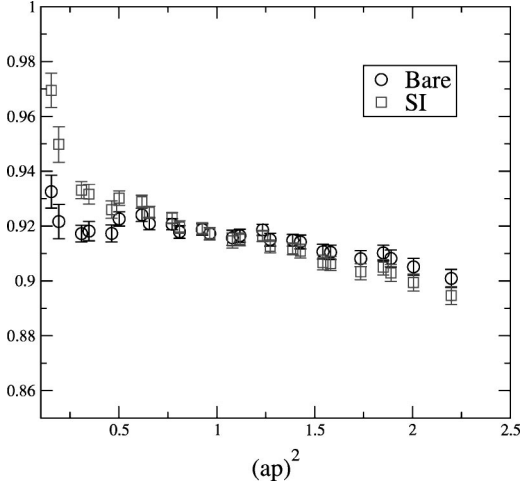
FIG. 14. A plot showing the raw data for $1/\Lambda_A$ (labeled as "Bare") and the value of $1/\Lambda_A$ divided by its predicted three loop perturbative running (labeled as "SI"), such that they coincide at $(ap)^2 = 1$, versus momentum. The slope of the latter versus $(ap)^2$ may be interpreted as an $\mathcal{O}(a^2)$ effect and is ≈ -0.02.

$$\frac{Z^{\mathrm{RI}}}{Z^{\overline{\mathrm{MS}}}} = 1 + \frac{\alpha_s}{4\pi} Z_0^{(1)\mathrm{RI}} + \frac{\alpha_s^2}{(4\pi)^2} Z_0^{(2)(\mathrm{RI})} + \cdots. \qquad (84)$$

For a consistent treatment this ratio need only be known to one less power of α_s than the running is known.

(iii) A lattice value for α_s. The value of α_s affects the scale dependence of both the matching and running for this calculation. For this work the value of α_s was calculated at three loops using a lattice value of Λ_{QCD} taken from Ref. [30] as

$$\Lambda_{QCD} = 238 \pm 19 \ \mathrm{MeV}. \qquad (85)$$

To do this consistently with the way the lattice treatment in Ref. [30] was performed, their value of $r_0 = 0.5$ fm was taken and converted into a lattice spacing using the results of Ref. [31]. For the dimensionful scales that we will quote, we set the physical scale through the rho mass computed with domain wall fermions [12], which for $\beta = 6.0$ gives

$$a = 0.520(11) \ \mathrm{GeV}^{-1}. \qquad (86)$$

Both Z_A and Z_V should be scale independent, but this is not the case for Z_q. Figure 14 shows both $1/\Lambda_A$ and the scale invariant (SI) quantity calculated as described above:

$$\Lambda_A^{SI}[(ap)^2] = \Lambda_A[(ap)^2]/C_A[(ap)^2]. \qquad (87)$$

The quantity C_A is determined through three loops using the anomalous dimension coefficients calculated in Refs. [32,4,27] as described in Appendix B. It is normalized so that $C_A(1) = 1$. As can be seen, in this case the renormalization group running actually goes in the opposite direction from the data. The scale dependence of these data, either predicted or actual, is, however, very small and a plausible explanation for this is an $(ap)^2$ error. Indeed, when a linear fit of the SI data versus $(ap)^2$ is performed, for $0.8 < (ap)^2 < 2.0$, the
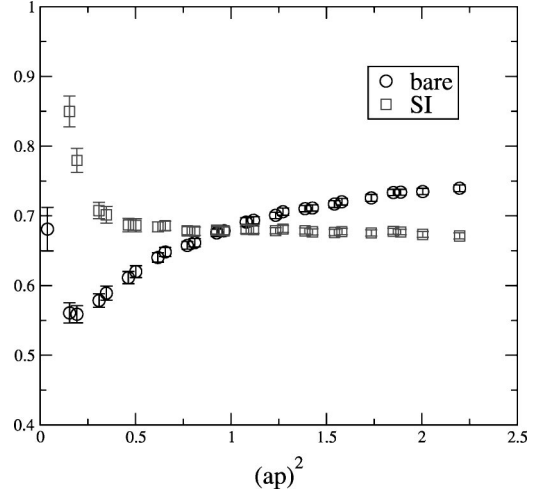

FIG. 15. A plot showing the raw data for $1/\Lambda_S$ (labeled as "Bare") and the value of $1/\Lambda_S$ divided by its predicted three loop perturbative running (labeled as "SI"), such that they coincide at $(ap)^2 = 1$, versus momentum. The slope of the latter versus $(ap)^2$ may be interpreted as an $\mathcal{O}(a^2)$ effect and is ≈ -0.003.

gradient is ≈ -0.02. A more compelling test of the renormalization group behavior is provided by studying the data for Z_S/Z_q. In this case the predicted scaling behavior over the range of momenta studied is much larger and, as Fig. 15 shows, the agreement between the predicted behavior and the data is impressive (with a gradient, in this case, of ≈ -0.003). The values for Z_S/Z_q versus momentum used here are taken after the mass-pole has been subtracted and, again, the three loop results for the running are taken from Refs. [32,4,27]. Unfortunately, a matching calculation for Z_T could not be found in the literature, so the data could only be compared to the one loop running (which is taken from Ref. [33]). The SI quantity so calculated is shown in Fig. 16 and has a gradient of ≈ -0.02.

Taking the interpretation that the remaining scale dependence is due to $\mathcal{O}[(ap)^2]$ effects, the correct way to extract the renormalization coefficients is to first construct the SI quantity as described above, and then fit any remaining scale dependence [4] to the form

$$y = c_1 + c_2(ap)^2, \qquad (88)$$

for a range of momenta that is chosen to be "above" the region for which condensate effects are deemed to be important. Table II shows the fitted values for the RI and $\overline{\mathrm{MS}}$ scheme renormalization coefficients using a fitting rage of $0.8 < (ap)^2 < 2.0$. Now that the renormalization group running has been taken into account, it is possible to make a comparison of the various methods of calculating Z_q and thus give final results for the renormalization factors. Table II already gives Z_q as calculated from the conserved currents (Fig. 17 shows the momentum dependence of both the SI and bare form; see also Table III). Another simple way to derive this quantity is by taking Z_A/Z_q from Table II and combining it with the value of Z_A obtained from hadronic matrix ele-
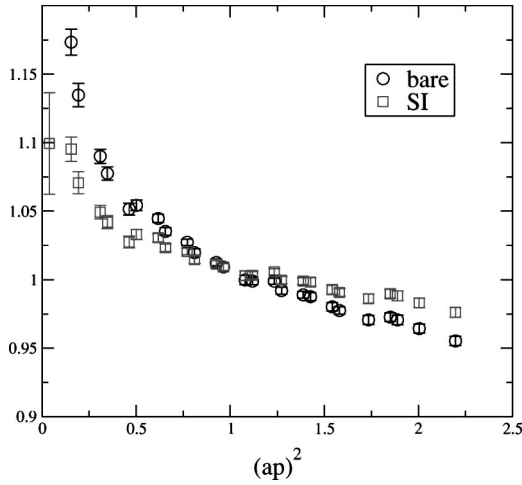
FIG. 16. A plot showing the raw data for $1/\Lambda_T$ (labeled as "Bare") and the value of $1/\Lambda_T$ divided by its predicted one loop perturbative running (labeled as "SI"), such that they coincide at $(ap)^2 = 1$, versus momentum. The slope of the latter versus $(ap)^2$ may be interpreted as an $\mathcal{O}(a^2)$ effect and is ≈ -0.02.

ments. This gives $Z_q = 0.805(3)(15)$. This, approximately 5%, difference may be taken as an indication of the size of the systematic errors.

XI. Z_q FROM THE PROPAGATOR—RESULTS

Here we show results for the wave function renormalization computed through Eq. (48) and demonstrate that this method contains a comparatively large systematic uncertainty due to the ambiguity in defining discrete momentum. We use the perturbative matching between Z_q' and Z_q, as given in Ref. [27].[1] Then the SI Z_q can be constructed as described above.

Figure 18 shows the SI Z_q using Z_q' defined in Eq. (48), and Fig. 19 shows the SI Z_q where the replacement

$$ap_\mu \rightarrow \sin(ap_\mu) \equiv a\bar{p}_\mu \qquad (89)$$

is made in Eq. (48). Note that the former is plotted vs $(ap)^2$ and the latter vs $(a\bar{p})^2$. We use the data at $m_f = 0.02$ since no mass dependence can be observed.

As in the previous section, we extrapolate to $(ap)^2 = 0$. We find for the data in Fig. 18, $Z_q = 0.715 \pm 0.007 \pm 0.040$, where the first error is statistical and the second comes from different choices for the range of momenta over which to fit. The data in Fig. 19 give $Z_q = 0.733 \pm 0.007 \pm 0.050$. We can further probe these discretization uncertainties by extrapolating Z_q^{-1} to zero $(ap)^2$ or $(a\bar{p})^2$. This results in $Z_q = 0.732 \pm 0.006 \pm 0.020$ and $Z_q = 0.772 \pm 0.006 \pm 0.020$, respectively.

The spread in values of Z_q obtained depending on momentum ranges and on the definition of discrete momenta means that extracting a SI Z_q in the same manner as the Z's

---

[1]Their convention is that a given Z factor in Ref. [27] is the reciprocal of ours.

TABLE II. Final Z-factor results. Z_q is calculated two ways: from using Z_A/Z_q from this table combined with Z_A from hadronic matrix elements, denoted Z_q^{Hadronic}, and from the conserved currents using off-shell quark states, denoted Z_q^{Ward}.

Z-factor	RI/SI	$\overline{\text{MS}}$ at 2 GeV
Z_A/Z_q	0.934 (2)(10)	0.938 (2)(12)
Z_S/Z_q	0.683 (7)(30)	0.779 (8)(35)
Z_T/Z_q	1.034 (3)(100)	1.035 (3)(100)
Z_q^{Hadronic}	0.808 (3)(15)	0.805 (3)(17)
Z_q^{Ward}	0.753 (16)(30)	0.750 (15)(30)

for bilinear operators is less precise. However, the results are in rough agreement with the more precise methods described above.

XII. COMPARISON WITH PERTURBATION THEORY

All the renormalization factors considered above have also been calculated in lattice perturbation theory, at the one loop level, for the domain wall fermion action in the $L_s \rightarrow \infty$ limit [20,19,21]. As we see little evidence of explicit chiral symmetry breaking effects in our study, the fact that the perturbative calculations have been performed in the $L_s \rightarrow \infty$ limit will probably not affect this comparison. However, a more serious issue is which M_5 value to use in the perturbative formulas.

The reason for this is easy to understand. Away from the walls, the massless domain wall fermion Lagrangian, Eq. (5), may be viewed as a simple extension of the standard Wilson fermion action to five dimensions with a negative mass term, M_5. Like the four dimensional Wilson mass term, M_5 undergoes a strong additive renormalization, the size of which perturbation theory is not good at predicting. While a more accurate prediction may be made using tadpole improved perturbation theory [2], a good deal of ambiguity remains in
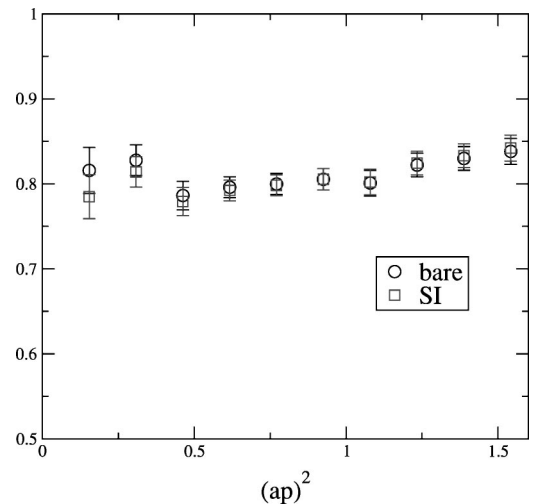

FIG. 17. Bare and scale invariant (SI) versions of Z_q determined from the conserved axial and vector currents.

TABLE III. This table collects together the raw data used for the "Bare" data plotted in Figs. 14, 15 and 16 for $0.5 < (ap)^2 < 2.0$.

$(ap)^2$	$1/\Lambda_A$	$1/\Lambda_S$	$1/\Lambda_T$
0.501	0.9225(26)	0.6200(86)	1.0542(38)
0.616	0.9240(23)	0.6401(67)	1.0446(30)
0.655	0.9208(22)	0.6481(64)	1.0352(28)
0.771	0.9206(20)	0.6574(55)	1.0273(22)
0.810	0.9178(23)	0.6614(59)	1.0197(27)
0.925	0.9187(21)	0.6755(53)	1.0125(25)
0.964	0.9172(22)	0.6784(54)	1.0092(24)
1.079	0.9157(27)	0.6910(62)	0.9997(34)
1.118	0.9164(23)	0.6935(52)	0.9989(26)
1.234	0.9185(20)	0.7007(45)	0.9989(23)
1.272	0.9150(23)	0.7059(51)	0.9920(26)
1.388	0.9147(21)	0.7102(45)	0.9889(24)
1.426	0.9141(25)	0.7112(45)	0.9876(29)
1.542	0.9106(26)	0.7168(48)	0.9801(30)
1.581	0.9104(25)	0.7202(48)	0.9775(27)
1.735	0.9080(29)	0.7257(49)	0.9706(32)
1.851	0.9101(28)	0.7334(45)	0.9727(31)
1.889	0.9081(30)	0.7339(42)	0.9706(35)

the perturbative prediction of any quantity that is strongly dependent on M_5.

Further consideration of the similarity of the domain wall and standard Wilson actions, leads to a nonperturbative estimate of the magnitude of this additive renormalization. As argued in Ref. [21], in the $L_s \to \infty$ limit, the effect of this additive renormalization may be taken into account by using

$$M_5^{\text{pert}} = M_5^{\text{sim}} - \left(4 - \frac{1}{2\kappa_c}\right), \quad (90)$$

in the perturbative equations, where κ_c is the four-dimensional critical Wilson hopping parameter and M_5^{sim} refers to the value used in the nonperturbative simulation (in

our case $M_5^{\text{sim}} = 1.8$). For $\beta = 6.0$, this ansatz leads to a shift of magnitude ≈ 0.8, which has been found to describe the dependence of the pion mass squared as a function of M_5 to a good degree of accuracy in a numerical simulation with $L_s = 14$ [21].

Equation (4.10) in Ref. [19] gives the complete one loop bilinear renormalization constants in the $\overline{\text{MS}}$ scheme:

$$Z_\Gamma^{\text{total}} = [(1 - w_0^2) Z_w]^{-1} Z_\Gamma. \quad (91)$$

Here Z_w, Z_2, and Z_Γ are to be computed from Eqs. (3.30), (3.42), and (4.11) and Tables II and III in Ref. [19], while $w_0 = 1 - M_5$. In the mean-field improved case, the above relations hold with the replacements $w_0 \to w_0^{MF} = w_0 + 4(1 - u)$, $Z_w \to Z_w^{MF}$, $Z_2 \to u Z_2^{MF}$, and $Z_\Gamma \to u Z_\Gamma^{MF}$ [34], whose values can also be computed from Tables II and III in Ref. [19]. The factor u in these formulas is the mean link variable in the Feynman gauge. As it is not possible to use the value of the mean link in the Feynman gauge, we have instead used the fourth root of the plaquette and the perturbative results of Ref. [17] to convert the results of Ref. [19].

In Fig. 20 and Fig. 21 we plot Z_A^{total} and Z_S^{total}, respectively, as functions of the variable M_5 in naive perturbation theory, in naive perturbation theory with the variable M_5 shifted according to Eq. (90) and in the mean-field improved case. To compute α_s, we used the same input values for Λ_{QCD} and a as in the perturbative running calculations in Sec. X. We obtain $\alpha_s[(ap)^2 = 1] = 0.20$. These figures show appreciable M_5 dependence. Our nonperturbative result is shown as a point corresponding to the single value of $M_5 = 1.8$ that we have studied.

The naive perturbation theory curve has a significant dependence on the precise value of α_s. In the mean-field improved case this problem is not as serious as the coefficient of α_s is a factor of 2–3 times smaller. Examining Figs. 20 and 21, one recognizes that naive perturbation theory does a poor job of determining Z_A or Z_S giving values nearly 2 times too small for $M_5 = 1.8$. Introducing the shift of Eq. (90) improves the situation noticeably giving values 15% too small and to within a few percent, although the perturbative
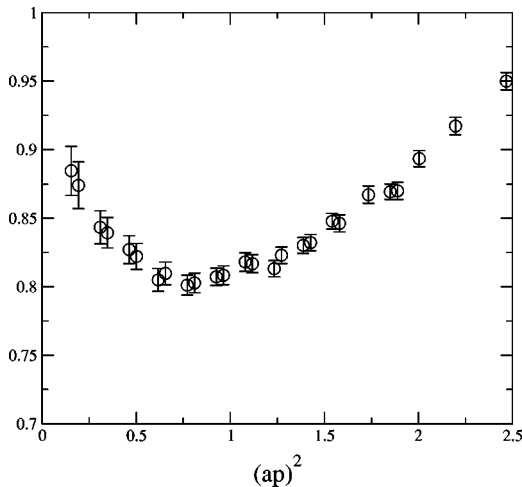

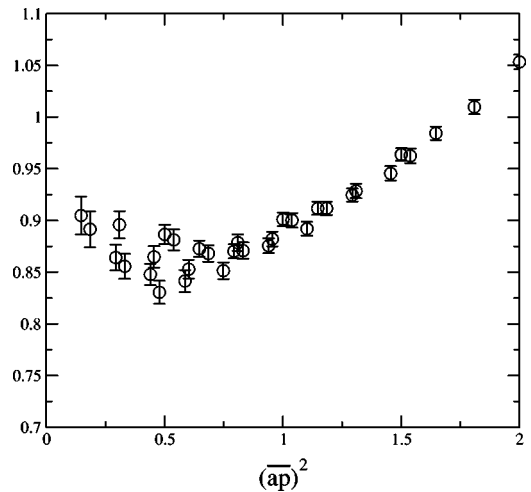FIG. 18. A scale invariant (SI) version of Z_q determined from Z'_q.

FIG. 19. The scale invariant (SI) version of Z_q determined from Z'_q but using $a\bar{p}_\mu$ instead of ap_μ.
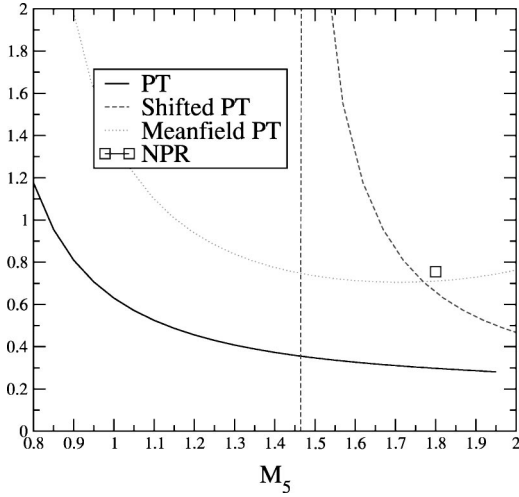
FIG. 20. The renormalization factor Z_A^{total} of Eq. (91) in the $\overline{\text{MS}}$ scheme at 2 GeV computed in naive perturbation theory, naive perturbation theory shifted by $(4 - 1/2\kappa_c)$ as in Eq. (90) and mean field improved perturbation theory.

result is rapidly varying with M_5 in this case. The mean-field results differ from the nonperturbative result by around 5% in both cases.

XIII. CONCLUSIONS

In this paper we have described a first study of non-perturbative renormalization of the quark field and flavor nonsinglet fermion bilinear operators in the context of domain wall fermions. We presented a theoretical argument constraining the form that explicit chiral symmetry breaking effects may take, and found that numerically these are insignificant, as might be expected from the measured size of the additive mass renormalization, m_{res} [12,13]. However, systematic effects due to spontaneous chiral symmetry breaking and zero-modes are significant, but accurately follow the expected form and can be effectively subtracted away.

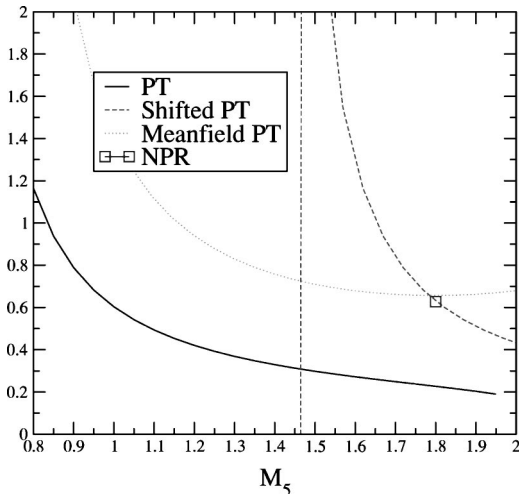Renormalization group invariant quantities were obtained

FIG. 21. Same as Fig. 20 but for Z_S^{total}.

in Sec. X by dividing the regularization independent scheme coefficients by the three loop renormalization group running (where available). The residual scale dependence of these quantities is small and was treated as an $\mathcal{O}(a^2)$ error. Three different quantities were used to determine the quark renormalization factor: the off-shell vertex functions of the conserved vector and axial currents; the trace of the product of $p^\mu \gamma^\mu$ and the off-shell quark propagator; and the combination of Z_A as determined from hadronic matrix elements with the value of Z_A/Z_q obtained in this study from the off-shell, axial vector vertex function. The technique of obtaining this Z_q directly from the propagator suffers from large discretization errors, but is roughly consistent with the other two methods which gave results differing by $\approx 5\%$.

In the final section we compared our results against the predictions of both standard and mean-field improved one loop perturbation theory.

APPENDIX A: THE RUNNING OF α_s

In the following the definitions

$$\alpha = \frac{g^2}{4\pi}, \tag{A1}$$

and

$$C_F = \frac{N_C^2 - 1}{2N_C}, \tag{A2}$$

will be used. The renormalized coupling may be defined in terms of the bare coupling by

$$\alpha_b = Z_g^2 \alpha_s \mu^{2\epsilon}. \tag{A3}$$

As α_b is completely independent of μ,

$$\mu^2 \frac{d\alpha_s}{d\mu^2} = -\epsilon\alpha_s + \beta \tag{A4}$$

with,

$$\beta = -\alpha_s \frac{2}{Z_g} \mu^2 \frac{dZ_g}{d\mu^2}. \tag{A5}$$

The results for the beta function are most easily given in terms of the β_i variable:

TABLE IV. β_i's for the quenched theory.

β_i	Quenched Value
β_0	11
β_1	102
β_2	1428.5

$$\frac{\beta(\alpha_s)}{4\pi} = -\beta_0\left[\frac{\alpha_s}{4\pi}\right]^2 - \beta_1\left[\frac{\alpha_s}{4\pi}\right]^3 - \dots. \qquad (A6)$$

The values used in the current work are summarized in Table IV. They are taken from Ref. [27] with the number of flavors set to zero (as we are working in the quenched case) and the number of colors set to three.

Once the β_i's are known, the running equation,

$$\mu\frac{d}{d\mu}\alpha_s = -2\beta_0\frac{\alpha_s^2}{4\pi} - 2\beta_1\frac{\alpha_s^3}{(4\pi)^2} - \dots, \qquad (A7)$$

may be solved.

One loop solution:

$$\frac{\alpha_s}{4\pi} = \frac{1}{\beta_0 \ln(\mu^2/\Lambda_{QCD}^2)}. \qquad (A8)$$

Two loop solution [35]:

$$\frac{\alpha_s}{4\pi} = \frac{1}{\beta_0 \ln(\mu^2/\Lambda_{QCD}^2)} - \frac{\beta_1 \ln\ln(\mu^2/\Lambda_{QCD}^2)}{\beta_o^3 \ln^2(\mu^2/\Lambda_{QCD}^2)}. \qquad (A9)$$

Three loop solution [4]:

$$\frac{\alpha_s}{4\pi} = \frac{1}{\beta_0 \ln(\mu^2/\Lambda_{QCD}^2)} - \frac{\beta_1 \ln\ln(\mu^2/\Lambda_{QCD}^2)}{\beta_o^3 \ln^2(\mu^2/\Lambda_{QCD}^2)}$$

$$+ \frac{1}{\beta_0^5 \ln^3(\mu^2/\Lambda_{QCD}^2)}\{\beta_1^2 \ln^2 \ln(\mu^2/\Lambda_{QCD}^2)$$

$$- \beta_1^2 \ln\ln(\mu^2/\Lambda_{QCD}^2) + \beta_2\beta_0 - \beta_1^2\}. \qquad (A10)$$

APPENDIX B: THE RUNNING OF THE Z-FACTORS

As mentioned previously, the renormalized operators we are working with are defined as

$$Z_O O_{bare} = O_{ren}. \qquad (B1)$$

TABLE V. Quenched Z_q anomalous dimensions.

Elements of γ_q	Quenched Value
$\gamma^{(0)}$	0
$\gamma^{(1)}$	44.6667
$\gamma^{(2)}$	1056.65

TABLE VI. Quenched Z_S anomalous dimensions.

Elements of γ_S	Quenched Value
$\gamma^{(0)}$	-8
$\gamma^{(1)}$	-134.667
$\gamma^{(2)}$	-2498

Requiring that the bare operator is independent of the renormalization scale gives the RG equation,

$$\mu^2\frac{d}{d\mu^2}O_{ren} = \frac{1}{Z_O}\mu^2\frac{dZ_O}{d\mu^2}O_{ren} \qquad (B2)$$

$$= -\frac{\gamma_O}{2}O_{ren}. \qquad (B3)$$

Writing the solution to this equation as

$$Z_O(\mu^2) = \frac{C_O(\mu'^2)}{C_O(\mu^2)}Z_O(\mu'^2), \qquad (B4)$$

and using the notation

$$\gamma_O = \sum_i \gamma_O^{(i)}\left(\frac{\alpha_s}{4\pi}\right)^{i+1} \qquad (B5)$$

$$\bar{\gamma}_{Oi} = \frac{\gamma_O^{(i)}}{2\beta_0} \qquad (B6)$$

$$\bar{\beta}_i = \frac{\beta_i}{\beta_0}, \qquad (B7)$$

gives rise to solutions to the running equation of the following form (where we have suppressed the subscripts identifying the particular operator O).

One loop solution [35]:

$$C(\mu^2) = \alpha_s(\mu)^{\bar{\gamma}_0}. \qquad (B8)$$

Two loop solution:

$$C(\mu^2) = \alpha_s(\mu)^{\bar{\gamma}_0}\left\{1 + \frac{\alpha_s(\mu)}{4\pi}(\bar{\gamma}_1 - \bar{\beta}_1\bar{\gamma}_0)\right\}. \qquad (B9)$$

Three loop solution:

TABLE VII. Quenched Z_T anomalous dimension.

Elements of γ_T	Quenched Value
$\gamma^{(0)}$	2.66667

TABLE VIII. Z_q RI to $\overline{MS}$ matching coefficients.

$Z_0^{(1)}$	0
$Z_0^{(2)}$	-14.4975

TABLE IX. Z_S RI to $\overline{MS}$ matching coefficients.

$Z_0^{(1)}$	5.33333
$Z_0^{(2)}$	188.651

$$
\begin{aligned}
C(\mu^2) = \alpha_s(\mu)^{\bar{\gamma}_0} & \left\{ 1 + \frac{\alpha_s(\mu)}{4\pi}(\bar{\gamma}_1 - \bar{\beta}_1 \bar{\gamma}_0) \right. \\
& + \frac{1}{2}\left(\frac{\alpha_s(\mu)}{4\pi}\right)^2 [(\bar{\gamma}_1 - \bar{\beta}_1 \bar{\gamma}_0)^2 + \bar{\gamma}_2 + \bar{\beta}_1^2 \bar{\gamma}_0 - \bar{\beta}_1 \bar{\gamma}_1 \\
& \left. - \bar{\beta}_2 \bar{\gamma}_0] \right\}.
\end{aligned} \tag{B10}
$$

Tables V–VII show the anomalous dimensions used in this work. These values were taken from Refs. [32,4,33] with the number of flavors set to zero and the number of colors to three.

APPENDIX C: MATCHING COEFFICIENTS

The numerical values of the matching coefficients, $Z_0^{(1)}$ and $Z_0^{(2)}$ in Eq. (84), used for Z_q and Z_S are collected together in Table VIII and Table IX.

[1] S. J. Brodsky, G. P. Lepage, and P. B. Mackenzie, Phys. Rev. D **28**, 228 (1983).

[2] G. P. Lepage and P. B. Mackenzie, Phys. Rev. D **48**, 2250 (1993).

[3] G. Martinelli, C. Pittori, C. T. Sachrajda, M. Testa, and A. Vladikas, Nucl. Phys. **B445**, 81 (1995).

[4] V. Gimenez, L. Giusti, F. Rapuano, and M. Talevi, Nucl. Phys. **B531**, 429 (1998).

[5] A. Donini, V. Gimenez, G. Martinelli, M. Talevi, and A. Vladikas, Eur. Phys. J. C **10**, 121 (1999).

[6] L. Giusti, V. Gimenez, F. Rapuano, M. Talevi, and A. Vladikas, Nucl. Phys. B (Proc. Suppl.) **73**, 210 (1999).

[7] D. Becirevic et al., Phys. Lett. B **444**, 401 (1998).

[8] JLQCD Collaboration, S. Aoki et al., presented at the XVI International Symposium on Lattice Field Theory LATTICE 98, 1998, Boulder, Colorado.

[9] D. B. Kaplan, Nucl. Phys. B (Proc. Suppl.) **30**, 597 (1993).

[10] Y. Shimir, Nucl. Phys. **B406**, 90 (1993).

[11] R. Narayanan and H. Neuberger, Nucl. Phys. **B443**, 305 (1995).

[12] T. Blum et al., Phys. Rev. D **65**, 014504 (2002).

[13] CP-PACS Collaboration, A. A. Khan et al., Phys. Rev. D **63**, 114504 (2001).

[14] M. L. Paciello, S. Petrarca, B. Taglienti, and A. Vladikas, Phys. Lett. B **341**, 187 (1994).

[15] M. Gockeler et al., Nucl. Phys. **B544**, 699 (1999).

[16] V. Furman and Y. Shamir, Nucl. Phys. **B439**, 54 (1995).

[17] S. Aoki, T. Izubuchi, Y. Kuramashi, and Y. Taniguchi, Phys. Rev. D **60**, 114504 (1999).

[18] S. Aoki and Y. Taniguchi, Phys. Rev. D **59**, 094506 (1999).

[19] S. Aoki, T. Izubuchi, Y. Kuramashi, and Y. Taniguchi, Phys. Rev. D **59**, 094505 (1999).

[20] S. Aoki and Y. Taniguchi, Phys. Rev. D **59**, 054510 (1999).

[21] T. Blum, A. Soni, and M. Wingate, Phys. Rev. D **60**, 114507 (1999).

[22] T. Blum, Nucl. Phys. B (Proc. Suppl.) **73**, 167 (1999).

[23] M. Bochicchio, L. Maiani, G. Martinelli, G. C. Rossi, and M. Testa, Nucl. Phys. **B262**, 331 (1985).

[24] D. Becirevic, V. Gimenez, V. Lubicz, and G. Martinelli, Phys. Rev. D **61**, 114507 (2000).

[25] H. D. Politzer, Nucl. Phys. **B117**, 397 (1976).

[26] P. Pascual and E. de Rafael, Z. Phys. C **12**, 127 (1982).

[27] E. Franco and V. Lubicz, Nucl. Phys. **B531**, 641 (1998).

[28] J.-R. Cudell, A. L. Yaouanc, and C. Pittori, Phys. Lett. B **454**, 105 (1999).

[29] T. Blum and S. Sasaki, hep-lat/0002019.

[30] ALPHA Collaboration, S. Capitani, M. Luscher, R. Sommer, and H. Wittig, Nucl. Phys. **B544**, 669 (1999).

[31] ALPHA Collaboration, M. Guagnelli, R. Sommer, and H. Wittig, Nucl. Phys. **B535**, 389 (1998).

[32] K. G. Chetyrkin and A. Retey, Nucl. Phys. **B583**, 3 (2000).

[33] H. He and X. Ji, Phys. Rev. D **52**, 2960 (1995).

[34] S. Aoki (private communication).

[35] A. J. Buras, hep-ph/9806471.